THE ASTROPHYSICAL JOURNAL, 297:413–422, 1985 October 15

FAST PULSARS: EFFECTS OF SPACETIME CURVATURE AND ROTATION ON THE PULSE CHARACTERISTICS

R. C. KAPOOR AND B. DATTA[1]
Indian Institute of Astrophysics, Bangalore
Received 1985 February 15; accepted 1985 April 23

ABSTRACT

The effects of spacetime curvature and rotation on the pulse profile of fast pulsars are studied using a rotationally perturbed spherical metric and a representative choice of the equation of state for neutron star matter. Spacetime curvature is found to produce a divergence in the pulse width and a deamplification of the pulse intensity. Rotation is found to produce an asymmetry in the final pulse profile accompanied by a tilt of the pulse cone axis from its original direction of emission. The astrophysical implications of these results pertaining to the pulse characteristics of fast pulsars are discussed.

Subject headings: pulsars — relativity

I. INTRODUCTION

The recent discovery of millisecond pulsars (Backer *et al.* 1982; Boriakoff, Buccheri, and Fauci 1983) has generated a lot of interest in the effect of rapid rotation on the structure of neutron stars and the various physical processes associated with such objects. The extremely rapid rotation rates of such pulsars pose the problem of their stability against breakup under centrifugal forces. The requirement of rotational stability would imply that these objects must be quite compact, having a large surface gravity (Datta and Ray 1983). An interesting consequence of rotation that has not been explored so far is the modifications, due to the general relativistic effect of dragging of inertial frames, in the trajectories of photons propagating near the pulsar. The large spacetime curvature (i.e., a large surface gravity) and large rotation are expected to lead to a modification in the pulse profile. In addition, rotation will introduce a certain amount of time delay in the arrival of photons and a reorientation of the plane of polarization (assuming it to be linear) of the pulse. The purpose of this paper is to present a detailed study of these effects with a view of applicability to the 1.5577 ms pulsar PSR 1937+214 and fast pulsars of this class. A preliminary summary of this work has appeared elsewhere (Datta and Kapoor 1985).

The Kerr solution, which is the full rotational analog to the spherically symmetric spacetime, does not have a corresponding appropriate interior solution amenable to a straightforward theoretical treatment. In this paper we use a rotationally perturbed interior spherical metric to take the rotational effects into account.

Our calculations suggest that the effect of spacetime curvature is to produce substantial amounts of divergence in the beam width of the emitted pulse and reduction in the pulse intensity. Rotation produces a tilt of the pulse cone axis (from its original direction of emission) and deforms the cone, leading effectively to an asymmetry in the flattened pulse profile. As a consequence of this, there will be a time delay in the arrival of photons emitted within the cone.

The format of the paper is as follows. Section II describes the rotationally perturbed geometry and the corresponding metric tensor. The calculations of photon trajectories in this rotationally perturbed spacetime are given in § III. Section IV describes the calculation of photon arrival times and the redshift factor (which is important in deciding the final pulse intensity distribution). The calculation of the final pulse profile is shown in § V. Section VI lists the choice of the equation of state of neutron star matter; and finally, the results and their implications pertaining to the pulse characteristics are given in § VII.

II. THE ROTATIONALLY PERTURBED GEOMETRY

The metric (signature: $+---$) we adopt to describe the rotationally perturbed spacetime, which also matches at the surface to an external metric, is (Hartle and Thorne 1968):

$$\begin{aligned} ds^2 &= g_{\alpha\beta}\,dx^\alpha dx^\beta\,, \quad (\alpha, \beta = 0, 1, 2, 3) \\ &= e^{2\nu}dt^2 - e^{2\psi}(d\phi - \omega dt)^2 \\ &\quad - e^{2\mu}d\theta^2 - e^{2\lambda}dr^2 + O(\Omega^3/\Omega_c{}^3)\,. \end{aligned} \tag{1}$$

Here Ω is the angular velocity of rotation and $\Omega_c = (M/R^3)^{1/2}$, where M and R are the mass and radius of the nonrotating neutron star. For the sake of simplicity, we put $c = 1 = G$. The metric components correspond to an interior with

$$e^{2\nu} = e^{2\Phi}\{1 + 2(h_0 + h_2 P_2)\}\,, \tag{2}$$

$$e^{2\psi} = r^2 \sin^2\theta\{1 + 2(v_2 - h_2)P_2\}\,, \tag{3}$$

$$e^{2\mu} = r^2\{1 + 2(v_2 - h_2)P_2\}\,, \tag{4}$$

$$e^{2\lambda} = \frac{1 + 2(m_0 + m_2 P_2)/(r - 2m)}{1 - 2m/r}\,, \tag{5}$$

and to an exterior with

$$e^{2\nu} = e^{-2\lambda} = 1 - 2M'/r + 2J^2/r^4\,, \tag{6}$$

$$e^{2\psi} = r^2 \sin^2\theta\,, \tag{7}$$

$$e^{2\mu} = r^2\,. \tag{8}$$

Here $M' = M + \delta M$, where δM is the rotationally induced mass deformation. The quantity P_2 is the Legendre polynomial of order 2, ω is the angular velocity of the cumulative dragging of inertial frames, and h_0, h_2, m_0, m_2, v_2 are all functions of r that are proportional to Ω^2. We retain only the spherical deformation terms characterized by subscript 0 and neglect the quadrupole deformation terms characterized by subscript 2

[1] Biren Roy Trust Fellow of the Indian National Science Academy.

(see Ray and Datta 1984). J is the angular momentum of the neutron star, given by

$$J = \frac{R^4}{6}\left(\frac{d\bar{\omega}}{dr}\right)_{r=R}, \tag{9}$$

where $\bar{\omega}(r) = \Omega - \omega(r)$ is determined from

$$\frac{d}{dr}\left(r^4 j \frac{d\bar{\omega}}{dr}\right) + 4r^3\bar{\omega}\frac{dj}{dr} = 0, \tag{10}$$

$$j(r) = e^{-\Phi(r)}(1 - 2m/r)^{1/2}, \tag{11}$$

$$\frac{d\Phi}{dr} = \frac{m + 4\pi r^3 P}{1 - 2m/r}, \tag{12}$$

with the boundary conditions

$$\Phi(\infty) = 0, \quad \left(\frac{d\bar{\omega}}{dr}\right)_{r=0} = 0, \quad \bar{\omega}(\infty) = \Omega. \tag{13}$$

Here m is the mass within a radius r, and P is the pressure at r.

The nonvanishing elements of the metric tensor are

$$g_{00} = e^{2\nu} - \omega^2 e^{2\psi}, \quad g_{11} = -e^{2\lambda}, \quad g_{22} = -e^{2\mu}, \quad g_{33} = -e^{2\psi}, \quad g_{03} = \omega e^{2\psi}. \tag{14}$$

The above prescription for the rotationally perturbed geometry is valid for strong gravitational fields but in the limit of uniform rotation with a rate that is slow compared to Ω_c, the critical speed for centrifugal break-up. Neutron star models rotating at the secular instability limit (Tassoul 1978)

$$\Omega_s = (0.27)^{1/2}\Omega_c \tag{15}$$

(assuming the star to be homogeneous) and relevant in the context of the millisecond pulsar PSR 1937+214 are within this bound.

III. PHOTON TRAJECTORIES IN THE ROTATIONALLY PERTURBED GEOMETRY

The four-velocity vector for the source of photon emission is

$$u^\alpha = \frac{dx^\alpha}{ds}, \quad x^\alpha = (t, r, \theta, \phi), \tag{16}$$

with

$$u^0 = dt/ds = e^{-\nu}(1 - v_s^2)^{-1/2}, \tag{17}$$

$$v_s = e^{\psi - \nu}(\Omega - \omega), \tag{18}$$

and

$$dr/ds = 0; \quad d\theta/ds = 0. \tag{19}$$

The quantity Ω, the angular velocity of the star as seen by a distant observer, is given by

$$d\phi/ds = \Omega dt/ds, \tag{20}$$

whereas v_s is the emitter's tangential velocity as seen by a locally nonrotating observer (so that $v_s = 1$ will correspond to the location of the light cylinder radius). The emitter describes a corotating circular orbit around the rotating star in the spacetime (eqs. [1], [6]–[8]).

Due to the rotation of the star, the trajectory of a photon emitted in a general direction from a point r_e will get dragged away from its original direction of emission *in addition* to getting bent due to spacetime curvature. The net angle of deflection in the trajectory will be given by (here Γ stands for affine parameter)

$$-\phi_0 = \int_{r_e}^{D} \frac{d\phi/d\gamma}{dr/d\Gamma}\, dr, \tag{21}$$

where D denotes the remote observer's location.

We denote the polar angle of emission made by the line of sight through the center of the star with respect to the axis of rotation by θ_s. So $\theta_s = 0$ will correspond to looking along the pole, and $\theta_s = \pi/2$, along the equator. Since we use a perturbed spherical metric, we can take θ_s to be approximately identical to the angle of inclination according to the remote observer, since the polar bending of the photon trajectory in the perturbed exterior Schwarzschild spacetime would be small as compared to the azimuthal bending. In other words, the photon emitted at the polar angle θ_s continues to move in the same plane passing through the center of the star.

The integral in equation (21) can be evaluated from a knowledge of the equations of motion of the photon corresponding to the external geometry using the Lagrangian technique.

The equations of motion are the Euler-Lagrange equations:

$$\frac{d}{d\Gamma}\left(\frac{\partial L}{\partial \dot{x}^\alpha}\right) - \frac{\partial L}{\partial x^\alpha} = 0, \tag{22}$$

where, for the metric (1),

$$L = \tfrac{1}{2}[e^{2\nu}\dot{t}^2 - e^{2\lambda}\dot{r}^2 - e^{2\mu}\dot{\theta}^2 - e^{2\phi}(\dot{\phi} - \omega\dot{t})^2]. \tag{23}$$

Here $x^\alpha = (t, r, \theta, \phi)$ and a dot represents derivative with respect to an affine parameter Γ. Equation (22), corresponding to the coordinates ϕ and t, gives respectively

$$g_{03}\dot{t} + g_{33}\dot{\phi} = -h, \tag{24}$$

$$g_{00}\dot{t} + g_{03}\dot{\phi} = \gamma, \tag{25}$$

where h and γ are constants of motion, identifiable respectively as the orbital angular momentum and the energy of the photon as measured by an observer situated at infinity. The ratio $q = -h/\gamma$ is finite and is defined as the impact parameter of the photon.

Equations (24) and (25) give

$$\frac{d\phi}{d\Gamma} = \frac{\gamma(g_{03} - qg_{00})}{g_{03}^2 - g_{00}g_{33}}, \tag{26}$$

$$\frac{dt}{d\Gamma} = \frac{\gamma(1 + \omega q)}{g_{00} + \omega g_{03}}. \tag{27}$$

For photons, the metric (1) is

$$0 = e^{2\nu}dt^2 - e^{2\lambda}dr^2 - e^{2\psi}(d\phi - \omega dt)^2. \tag{28}$$

That gives

$$\frac{dr}{d\Gamma} = e^{\nu-\lambda}\frac{dt}{d\Gamma}[1 - e^{2\psi-2\nu}(x-\omega)^2]^{1/2}, \tag{29}$$

where

$$x = \frac{d\phi/d\Gamma}{dt/d\Gamma} = -\frac{g_{03} - qg_{00}}{g_{33} - qg_{03}}$$
$$= \omega - \frac{qe^{2\nu}}{e^{2\psi}(1+\omega q)}. \tag{30}$$

The deflection angle (21) then becomes a function of the radial emission coordinate and the impact parameter

$$-\phi_0 = \int_{r_e}^{D} f(r, q_e)dr, \tag{31}$$

where

$$f(r, q_e) = -\frac{g_{03} - q_e g_{00}}{(1+\omega q_e)g_{33}e^{\nu-\lambda}[1 - e^{2\psi-2\nu}(x-\omega)^2]^{1/2}}$$
$$= \frac{\omega(1+\omega q_e) - q_e e^{2\nu-2\psi}}{e^{\nu-\lambda}[(1+\omega q_e)^2 - q_e{}^2 e^{2\nu-2\psi}]^{1/2}}, \tag{32}$$

with

$$q_e \equiv q(r = r_e, \theta_s, \delta). \tag{33}$$

It is convenient to derive the value of the impact parameter in the frame of reference of a locally nonrotating observer, that is, one having the coordinates (r, θ) fixed and rotating with a coordinate angular velocity $\omega = d\phi/dt$. A Lorentz transformation to the frame of reference of the emitter then gives (Kapoor and Datta 1984):

$$q_e = \left.\frac{e^{\psi-\nu}(v_s + \sin\delta)}{1 + e^{\psi-\nu}(\omega v_s + \Omega\sin\delta)}\right|_{r=r_e}, \tag{34}$$

where δ is the azimuthal angle at which the photon is emitted with respect to the radius vector of the source through the origin of the system of coordinates as seen in the local rest frame of the star. It increases in the direction opposite to that of motion of the source. In the local rest frame, we choose the azimuthal angle such that $\delta = 0$ for a radially outgoing photon, and $\delta = 3\pi/2$ for a tangentially forward photon. It may be noted that not from all points on the circular orbit would the photon, emitted at a particular value of δ, be received by the remote observer. The value (34) for the impact parameter has been obtained by requiring that there will exist a certain point P from where the photon will reach the remote observer.

IV. PHOTON ARRIVAL TIMES AND REDSHIFTS

The times of emission and reception (at the remote observer) of a photon are determined in the manner described below. Consider a photon emitted from P at $t = t_0$. In order for the photon to arrive at the observer at Q at $t = T$,

$$T - t_0 = \int_{r_e}^{D}\frac{dt/d\Gamma}{dr/d\Gamma}dr$$
$$= \int_{r_e}^{D} g(r, q_e)dr, \tag{35}$$

where

$$g(r, q_e) = e^{\lambda-\nu}[1 - e^{2\psi-2\nu}(x-\omega)^2]^{1/2}$$
$$= \frac{1+\omega q_e}{e^{2\nu}[(1+\omega q_e)^2 - q_e{}^2 e^{2\nu-2\psi}]^{1/2}}. \tag{36}$$

Although the amount of deflection will be small for small values of the azimuthal angle, a *finite* time delay will be introduced between two neighboring null geodesics with δ and $\delta + d\delta$, which cannot be neglected. The implications of this fact will be discussed in § VII.

Closely connected with the above is the photon redshift factor. Consider now another photon emitted from the circular orbit at a world point P' with the time coordinate $t_0 + \Delta t_0$. This photon will arrive at Q at a time $T + \Delta T$ with an impact parameter $q_e + \Delta q_e$. A similar set of equations as before can be written for this photon also, so that we have

$$\Delta T - \Delta t_0 = \Delta q_e \int_{r_e}^{D}(\partial g/\partial q_e)dr, \tag{37}$$

where

$$\partial g/\partial q_e = q_e e^{-2\psi}[(1+\omega q_e)^2 - e^{2\nu-2\psi}q_e{}^2]^{-3/2} \tag{38}$$

and

$$-\Delta\phi_0 = \Delta q_e \int_{r_e}^{D}(\partial f/\partial q_e)dr. \tag{39}$$

Since

$$\Delta t_0/\Delta s = u^0 \tag{40}$$

and

$$\Delta\phi_0/\Delta s = \Omega u^0, \tag{41}$$

equations (37) and (39) give

$$\frac{\Delta T - u^0\Delta s}{(-\Omega u^0\Delta s)} \equiv H(q_e) = \frac{\int_{r_e}^{D}(\partial g/\partial q_e)dr}{\int_{r_e}^{D}(\partial f/\partial q_e)dr}, \tag{42}$$

$$\Delta T/\Delta s = u^0[1 - \Omega H(q_e)]. \tag{43}$$

Equation (43) gives the photon redshift factor and is equivalent to the expression for the redshift factor of rotating neutron stars reported earlier in Kapoor and Datta (1984) with the following identifications:

$$\Delta T/\Delta s = 1 + z = \nu_0/\nu, \tag{44}$$

$$H(q_e) = -q_e. \tag{45}$$

Here ν_0 and ν refer respectively to the frequencies of radiation at the source and the observer. Apart from time delay, redshift factor plays a nontrivial role in determining the final pulse profile.

V. THE PULSE PROFILE

From the preceding section, it follows that the effect of spacetime curvature will be to produce a divergence in the beam width of the pulse. Furthermore, the dragging of inertial frames brought on by rotation will deflect photon trajectories in the direction of rotation by an amount that is a function of the azimuthal angle at the emission location. This implies two things. First, there will be a tilt of the pulse cone axis from its original position. Second, there will be an overall asymmetry in the final pulse profile because, as can be seen from equation (34), the impact parameter is not symmetric in $\pm\delta$. This asym-

metry will, in principle, manifest itself in the observed pulse intensity distribution.

To make explicit the pulse divergence effect, let us assume that the axis of the cone of emission is directed radially away (that is, $\delta = 0$) from the pulsar's surface in the frame of reference of the emitter. Figure 1 shows schematically the deflection ϕ_0 sufferered by a photon trajectory. The new value of δ is denoted by $\delta_{\rm new}$, so that

$$\phi_0 = \delta_{\rm new} - \delta + \alpha \,, \tag{46}$$

where α is given by

$$\tan \alpha = -\left(r \frac{d\phi}{dr}\right)_{r=D} \,; \tag{47}$$

here $r = D$ specifies the location of the observer from the center of the pulsar, and $d\phi/dr$ is given by equation (31). To see the role of the impact parameter in determining the deflection, let us transform to a locally Cartesian set of coordinates at the observer. Since rotational effects decrease with distance much more rapidly that curvature effects, we can set $\theta_s \approx \pi/2$; then

$$\frac{d\phi}{dr} \approx \frac{q}{D^2} \,. \tag{48}$$

The largest deflection will thus correspond to the case $\delta = \pi/2$, when q attains its maximum value. In real astrophysical situations, $D \gg R$ and $\delta \ll 1$, so that we can approximate equation (47) by

$$(\tan \alpha)_{\rm max} \approx 0 \,. \tag{49}$$

Therefore,

$$\delta_{\rm new} = \delta + \phi_0(\delta) \,. \tag{50}$$

As a measure of the divergence effect, we introduce a parameter Δ, which we define as

$$\begin{aligned} \Delta &= \Delta(\delta, r_e) \\ &= \left(\frac{d\delta_{\rm new}}{d\delta}\right)_{r=r_e} \\ &= \left(1 + \frac{d\phi_0}{d\delta}\right)_{r=r_e} \,. \end{aligned} \tag{51}$$

This is an integro-differential equation where $d\phi_0/d\delta$ is determined from equation (31). As a consequence of rotation,

$$\Delta(\delta, r) \neq \Delta(-\delta, r) \,.$$

This is unlike the case of the spherically symmetric Schwarzschild spacetime, where although the spacetime curvature will produce the beam divergence effect of similar extent, the symmetry in $\pm\delta$ is maintained. This can be easily seen if one approximates the corresponding Schwarzschild expression of equation (21) as follows:

$${\phi_0}^{\rm S} \approx -\frac{q^{\rm S}}{R}\left[1 + \frac{\sin^2 \delta(2R - 3m^{\rm S})}{12(R - 2m^{\rm S})}\right] , \tag{52}$$

where the superscript S refers to the Schwarzschild case. Here $\theta = \pi/2$ for reasons of symmetry, and

$$q^{\rm S} = (e^{\psi - \nu} \sin \delta)_{r=R} \,, \tag{53}$$

$$m^{\rm S} = 2GM/c^2 \,. \tag{54}$$

Going back to the rotational case, it can be noticed that $\Delta \rightarrow 1$ as $\delta \rightarrow \pm\pi/2$, implying that for tangential emission, the divergence effect will be very small.

The phenomenon of the pulse beam divergence, as outlined above, has the important implication that the pulsar will, in effect, behave as a diverging lens for its own radiation. As a result, there will be a reduction in the intensity, which can be understood in terms of the conservation of the energy flux. We write the intensity deamplification factor as ϵ:

$$\begin{aligned} \epsilon &= \frac{I(\delta_{\rm new})}{I(\delta)} \\ &= \frac{1}{\Delta}\frac{\sin \delta}{\sin \delta_{\rm new}} \,. \end{aligned} \tag{55}$$

For emission close to the cone axis,

$$\epsilon(\delta \rightarrow 0) \approx \frac{1}{\Delta}\frac{\delta}{\delta_{\rm new}} = \frac{1}{\Delta^2} \,. \tag{56}$$

In determining the final pulse profile, correction must be made due to Doppler boosting (and diminution) effect. From Liouville's theorem, the observed specific intensity I_ν is related

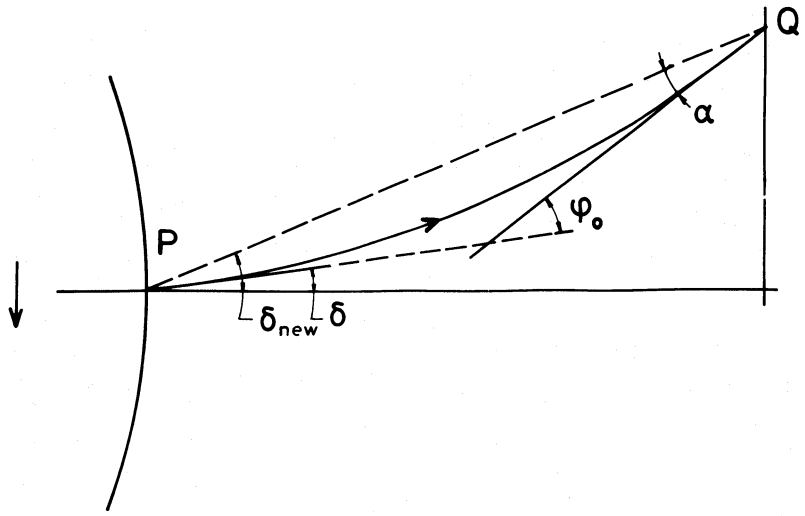

FIG. 1.—Schematic illustration of the photon trajectory in terms of the angles δ, ϕ_0, and $\delta_{\rm new}$

to the emitted monochromatic specific intensity I_{ν_0} (at a given δ) by

$$I_\nu = I_{\nu_0}(\nu/\nu_0)^3 = I_{\nu_0}(1+z)^{-3}\,, \tag{57}$$

where $(1+z)$ is the redshift factor given by equation (44). The redshift correction to intensity through a factor $[1+z(\delta=0)]^{-3}$ is inherent to the pulse. Over and above this, the intensity will get enhanced for photons emitted in the forward direction (i.e., for $\delta<0$) and reduced for photons emitted in the backward direction (i.e., for $\delta>0$). We define a net deamplification factor ϵ', which corrects ϵ for Doppler boosting (for $\delta<0$) and diminution (for $\delta>0$) as

$$\epsilon' = \epsilon\left\{\frac{1+z(0)}{1+z(\delta)}\right\}^3\,, \tag{58}$$

in accordance with Liouville's theorem. For fast pulsars such as PSR 1937+214, the quantity v_s will be a significant fraction of unity. Hence, the correction due to Doppler boosting will be nontrivial.

VI. CHOICE OF THE EQUATION OF STATE

The structure of neutron stars depends sensitively on the equation of state of neutron matter at high densities, especially around $\rho \approx 10^{15}$ g cm^{-3}. In this paper we have chosen the following five equations of state based on representative choices of neutron and nuclear matter interactions. These are: (1) the Reid-Pandharipande (RP) model, (2) the Bethe-Johnson (BJ) model I, (3) the tensor interaction (TI) model (for a detailed discussion of these see Pandharipande, Pines, and Smith 1976), (4) the Canuto-Datta-Kalman (CDK) model, which includes the short-range interaction due to nucleon-nucleon f^0-meson exchange ($f^2 = 2.91$ case) (Canuto, Datta, and Kalman 1978), and (5) the Friedman-Pandharipande (FP) model, which is based on an improved nuclear interaction that fits adequately two-nucleon scattering data and known nuclear matter properties (Friedman and Pandharipande 1981). The details regarding the composite equation of state and the corresponding rotating neutron star models are given in Ray and Datta (1984).

VII. RESULTS AND DISCUSSION

Analysis of available binary pulsar data is consistent with a neutron star mass in the range $(1.4 \pm 0.2)\ M_\odot$, $M_\odot$ = solar mass (Joss and Rappaport 1984). So, although no reliable mass estimates are available for the recently discovered fast pulsars, we adopt here the above value as the representative mass for the purpose of illustrating the effects of spacetime curvature and rotation on the pulse profile, taking PSR 1937+214 as the example. For this pulsar $\Omega = 4.0334 \times 10^3$ rad s^{-1}; the relevant parameters for the present calculations are listed in Table 1 (see Ray and Datta 1984 for details). Since PSR 1937+214 is close to the point of secular rotational instability, the results presented here may be taken to be indicative of the maximal effects of rotation.

There does not exist at present a general consensus on the pulse emission mechanism. The proposed mechanisms can be classified according to their location with respect to the neutron star. In this paper we choose one of the more influential models, namely, the one in which the emission is assumed to take place in the vicinity of the neutron star's surface in the form of a narrow conical beacon which rotates with the neutron star (Radhakrishnan and Cooke 1969), sweeping the pattern past the observer with a width ($\lesssim 10°$) that should be constant over many decades of frequency.

The theoretical framework presented in §§ III–V is general and will apply to *any* emission model and initial pulse profile. For the purpose of illustration, we take the initial pulse profile to be a steep Gaussian, with the range $-5° \le \delta \le 5°$. The mass (M') and radius (R') that enter the calculations refer to the *rotating* neutron star configurations, reported earlier in Ray and Datta (1984). The bending of photon trajectories and the final pulse profile have been calculated for various values of the polar emission angle θ_s, for each of the equations of state, and for $r_e = R'$, $2R'$, and $3R'$. The integrals occurring in equations (31), (35), and (51) have been evaluated numerically; an upper limit of $r = 700R'$ is found to be sufficient for this purpose.

The main conclusion that emerges from our calculations is this: the pulse cone width becomes divergent (we indicate this by the index Δ) by a factor ~ 2. These are illustrated in Tables 2–6 (for several values of θ_s) corresponding to the various equations of state. Besides Δ, the tables list the values $\delta_{\rm new}$ and ϵ'. The relative variations of the parameters over the different equations of state is not significant. So, from this consideration alone, it is not possible to discriminate among the equations of state. These tables also include the corresponding values for the Schwarzschild case and so facilitate a comparison between the two cases. The comparison indicates that the effect of rotation is small, and the spacetime curvature effect predominates. It should be noted that in Schwarzschild case, any plane is $\theta_s = \pi/2$ plane, and there is no functional dependence on θ_s as it is understood in the rotational case.

Figure 2 shows the final pulse profile, for different values of θ_s, $r_e = R'$ and corresponding to the FP model, which is believed to be the most realistic equation of state available. Figure 3 is the same as Figure 2, but it shows a comparison for different choices of r_e, keeping θ_s fixed ($=\pi/2$).

It may be noticed that the bending of photon trajectories is almost linear in δ. This can be easily seen to follow (for small δ) from equation (32) by noting that $\omega q_e \ll 1$ and $q_e \ll r_e$ and making a binomial expansion of the right-hand side.

The asymmetry introduced in the pulse profile by the drag-

TABLE 1

BULK PROPERTIES OF PSR 1937+214

Equation of State	$M'/M_\odot$	$M/M_\odot$	R' (10^6 cm)	R (10^6 cm)	J (10^{48} g cm^2 s^{-1})	$\bar{\omega}(R)$ (10^3 s^{-1})
RP	1.383	1.285	1.029	1.002	6.084	5.859
FP	1.416	1.308	1.119	1.087	6.492	5.285
CDK	1.423	1.305	1.176	1.141	6.675	4.939
BJ	1.399	1.301	1.323	1.281	6.105	4.274
TI	1.390	1.270	1.691	1.629	6.636	3.015

NOTE.—Mass $\approx 1.4\ M_\odot$; on the verge of secular rotational instability.

TABLE 2

RP MODEL

δ	δ_{new} +	δ_{new} −	Δ +	Δ −	ϵ' +	ϵ' −
Rotational Case						
$\theta_s = 0.3\pi$:						
0°	0°	0°	2.545	2.545	0.154	0.154
1	2.543	−2.547	2.540	2.549	0.154	0.155
2	5.080	−5.099	2.535	2.554	0.153	0.156
3	7.613	−7.656	2.531	2.559	0.153	0.157
4	10.142	−10.218	2.526	2.565	0.152	0.158
5	12.666	−12.785	2.522	2.570	0.152	0.159
$\theta_s = 0.5\pi$:						
0°	0°	0°	2.240	2.240	0.199	0.199
1	2.237	−2.242	2.235	2.245	0.198	0.201
2	4.470	−4.489	2.230	2.249	0.197	0.202
3	6.698	−6.741	2.226	2.254	0.196	0.203
4	8.921	−8.998	2.221	2.259	0.196	0.205
5	11.140	−11.259	2.217	2.265	0.195	0.206
Schwarzschild Case						
$\theta_s = 0.5\pi$:						
0°	0°	0°	2.252	2.252	0.197	0.197
1	2.252	−2.252	2.252	2.252	0.197	0.197
2	4.504	−4.504	2.252	2.252	0.197	0.197
3	6.756	−6.756	2.252	2.252	0.197	0.197
4	9.008	−9.008	2.252	2.252	0.197	0.197
5	11.260	−11.260	2.253	2.253	0.197	0.197

TABLE 3

FP MODEL

δ	δ_{new} +	δ_{new} −	Δ +	Δ −	ϵ' +	ϵ' −
Rotational Case						
$\theta_s = 0.3\pi$:						
0°	0°	0°	2.512	2.512	0.158	0.158
1	2.509	−2.514	2.507	2.517	0.158	0.159
2	5.014	−5.034	2.503	2.522	0.157	0.160
3	7.515	−7.558	2.498	2.527	0.157	0.161
4	10.010	−10.087	2.494	2.532	0.156	0.162
5	12.502	−12.621	2.489	2.537	0.156	0.164
$\theta_s = 0.5\pi$:						
0°	0°	0°	2.213	2.213	0.204	0.204
1	2.210	−2.215	2.208	2.217	0.203	0.206
2	4.416	−4.435	2.203	2.222	0.202	0.207
3	6.617	−6.659	2.199	2.227	0.201	0.209
4	8.813	−8.889	2.194	2.232	0.200	0.210
5	11.005	−11.124	2.190	2.237	0.199	0.212
Schwarzschild Case						
$\theta_s = 0.5\pi$:						
0°	0°	0°	2.226	2.226	0.202	0.202
1	2.226	−2.226	2.226	2.226	0.202	0.202
2	4.453	−4.453	2.226	2.226	0.202	0.202
3	6.679	−6.679	2.227	2.227	0.202	0.202
4	8.906	−8.906	2.227	2.227	0.202	0.202
5	11.133	−11.133	2.227	2.227	0.203	0.203

TABLE 4

CDK MODEL

δ	δ_{new} +	δ_{new} −	Δ +	Δ −	ϵ' +	ϵ' −
Rotational Case						
$\theta_s = 0.3\pi$:						
0°	0°	0°	2.490	2.490	0.161	0.161
1	2.488	−2.493	2.486	2.495	0.160	0.162
2	4.971	−4.990	2.481	2.500	0.160	0.163
3	7.450	−7.493	2.476	2.505	0.159	0.164
4	9.924	−10.000	2.472	2.510	0.159	0.165
5	12.394	−12.513	2.468	2.515	0.158	0.167
$\theta_s = 0.5\pi$:						
0°	0°	0°	2.195	2.195	0.208	0.208
1	2.192	−2.197	2.190	2.200	0.206	0.209
2	4.380	−4.399	2.186	2.204	0.205	0.210
3	6.563	−6.606	2.181	2.209	0.204	0.212
4	8.742	−8.818	2.176	2.214	0.203	0.214
5	10.916	−11.034	2.172	2.219	0.202	0.216
Schwarzschild Case						
$\theta_s = 0.5\pi$:						
0°	0°	0°	2.209	2.209	0.205	0.205
1	2.209	−2.209	2.209	2.209	0.205	0.205
2	4.418	−4.418	2.209	2.209	0.205	0.205
3	6.627	−6.627	2.209	2.209	0.205	0.205
4	8.837	−8.837	2.209	2.209	0.206	0.206
5	11.046	−11.046	2.210	2.210	0.206	0.206

TABLE 5

BJ MODEL

δ	δ_{new} +	δ_{new} −	Δ +	Δ −	ϵ' +	ϵ' −
Rotational Case						
$\theta_s = 0.3\pi$:						
0°	0°	0°	2.436	2.436	0.169	0.169
1	2.434	−2.438	2.432	2.441	0.168	0.170
2	4.863	−4.882	2.427	2.446	0.167	0.171
3	7.288	−7.329	2.423	2.450	0.166	0.172
4	9.708	−9.782	2.418	2.455	0.165	0.173
5	12.124	−12.240	2.414	2.460	0.165	0.175
$\theta_s = 0.5\pi$:						
0°	0°	0°	2.150	2.150	0.216	0.216
1	2.148	−2.153	2.146	2.155	0.215	0.218
2	4.292	−4.310	2.141	2.160	0.213	0.220
3	6.431	−6.472	2.137	2.164	0.212	0.221
4	8.565	−8.639	2.133	2.169	0.211	0.223
5	10.696	−10.810	2.128	2.174	0.210	0.225
Schwarzschild Case						
$\theta_s = 0.5\pi$:						
0°	0°	0°	2.174	2.174	0.212	0.212
1	2.174	−2.174	2.174	2.174	0.212	0.212
2	4.347	−4.347	2.174	2.174	0.212	0.212
3	6.521	−6.521	2.174	2.174	0.212	0.212
4	8.695	−8.695	2.174	2.174	0.212	0.212
5	10.869	−10.869	2.174	2.174	0.213	0.213

TABLE 6

TI MODEL

δ	δ_{new} +	δ_{new} −	Δ +	Δ −	ϵ' +	ϵ' −
TI Model Rotational Case						
$\theta_s = 0.3\pi$:						
0°	0°	0°	2.353	2.353	0.181	0.181
1	2.351	−2.355	2.348	2.358	0.179	0.182
2	4.696	−4.716	2.343	2.363	0.178	0.183
3	7.037	−7.081	2.338	2.368	0.177	0.185
4	9.373	−9.452	2.334	2.374	0.176	0.187
5	11.704	−11.828	2.329	2.379	0.176	0.188
$\theta_s = 0.5\pi$:						
0°	0°	0°	2.080	2.080	0.231	0.231
1	2.077	−2.082	2.075	2.085	0.229	0.233
2	4.150	−4.170	2.070	2.090	0.228	0.235
3	6.218	−6.262	2.065	2.095	0.226	0.238
4	8.281	−8.360	2.061	2.100	0.224	0.240
5	10.339	−10.463	2.056	2.106	0.223	0.243
Schwarzschild Case						
$\theta_s = 0.5\pi$:						
0°	0°	0°	2.114	2.114	0.224	0.224
1	2.114	−2.114	2.114	2.114	0.224	0.224
2	4.228	−4.228	2.114	2.114	0.224	0.224
3	6.341	−6.341	2.114	2.114	0.224	0.224
4	8.455	−8.455	2.114	2.114	0.224	0.224
5	10.569	−10.569	2.114	2.114	0.225	0.225

NOTE TO TABLES 2–6.—Azimuthal bending, divergence index Δ, and deamplification factor ϵ' corresponding to the model rotational cases and the Schwarzschild case (emission taken at the pulsar surface).

ging of inertial frames due to rotation is brought out by the index Δ. The pulse profile gets deformed in the direction of rotation, the cone becoming compressed for the backward emission (i.e., for $\delta > 0$) and stretched for the forward emission (i.e., for $\delta < 0$). The deformation is not uniform; it increases as one goes from backward to forward emission angles. The deformation extent, however, is small and is more clearly discernible in Tables 2–6 than in Figures 2 and 3.

The factor ϵ increases as one moves away from the pulse cone axis. As distinct from ϵ, the net deamplification factor ϵ' has a decreasing trend in $\delta(>0)$ (calculated here for $\theta_s = 0.3\pi$ and 0.5π; see Tables 2–6). For the case of the forward emission ($\delta < 0$), there is a reversal of the above trend. The importance of Doppler boosting (or diminution, as the case may be), no matter its actual magnitude for the range of δ considered here, is thus clearly discernible. Figure 4 gives a plot of ϵ' as a function of r_e for the rotational as well as the Schwarzschild case (for which $\epsilon' = \epsilon$ and is symmetric in $\pm\delta$).

Another interesting result of our calculations is the "sweeping" of the entire pulse cone in the direction of rotation of the pulsar, thus imparting a tilt to the cone. The tilt is to be understood in terms of the net bending suffered by a $\delta = 0$ (i.e., radial outward) photon. An analytic expression for the tilt angle (for $\omega q_e \ll 1$ and $q_e \ll r_e$), is

$$-\phi_0(\delta = 0) = \int_{r_e}^{D} \frac{\omega dr}{e^{2\nu}} - \int_{r_e}^{D} \frac{dr}{r^2}\left[\frac{r^2(\Omega - \omega)}{e^{2\nu}(1 + \omega v_s e^{\psi - \nu})}\right]_{r=r_e} . \quad (59)$$

Table 3 gives the amount of tilt as well as time delay for backward- and forward-emitted photons for all the equations of state used here and for various values of r_e. We find that $\Delta > 1$, even at $r_e \approx 0.8R_L$ (R_L = light cylinder radius), indicating that the beam divergence effect (for normally radiated emission) extends almost to the light cylinder radius. The effect, however, is essentially unimportant for the relativistic beam model, in which case $\Delta \approx 1$ for $\delta \approx \pm\pi/2$.

In view of the high degree of linear polarization in the emission from many pulsars, it is worth mentioning the rotation of the plane of polarization due to the dragging of inertial frames. Since an inertial compass near the surface of a rotating neutron star precesses with an angular velocity ω, the plane of polarization will rotate with the same velocity (Zeldovich and

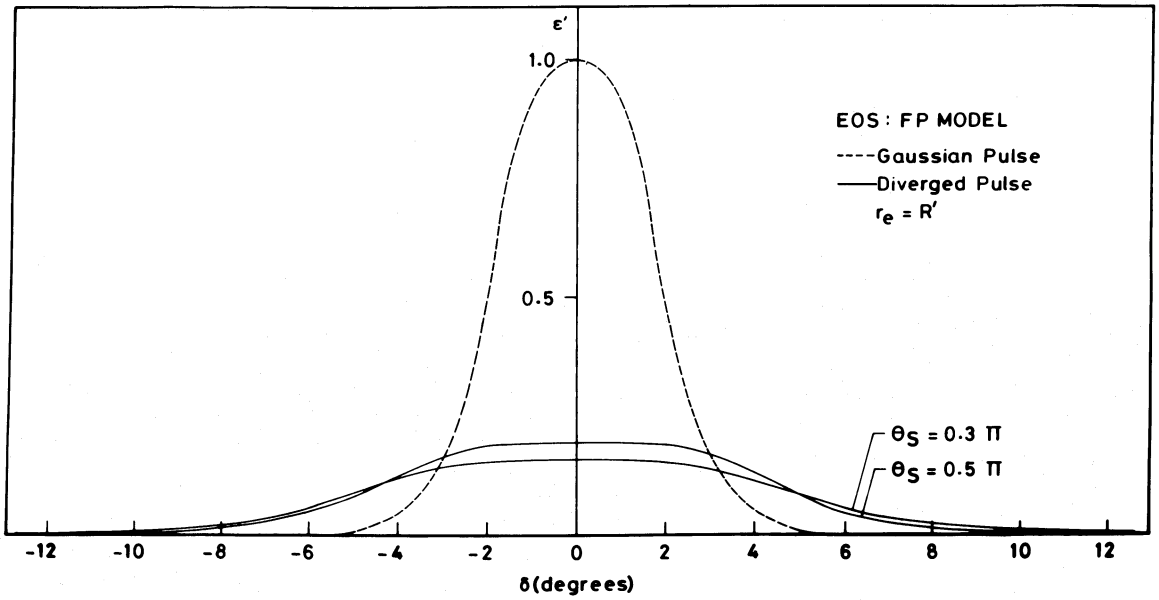

FIG. 2.—Net deamplification factor ϵ' vs. azimuthal angle for two values of θ_s (*solid curves*). The dashed curve corresponds to the initial (Gaussian) profile.

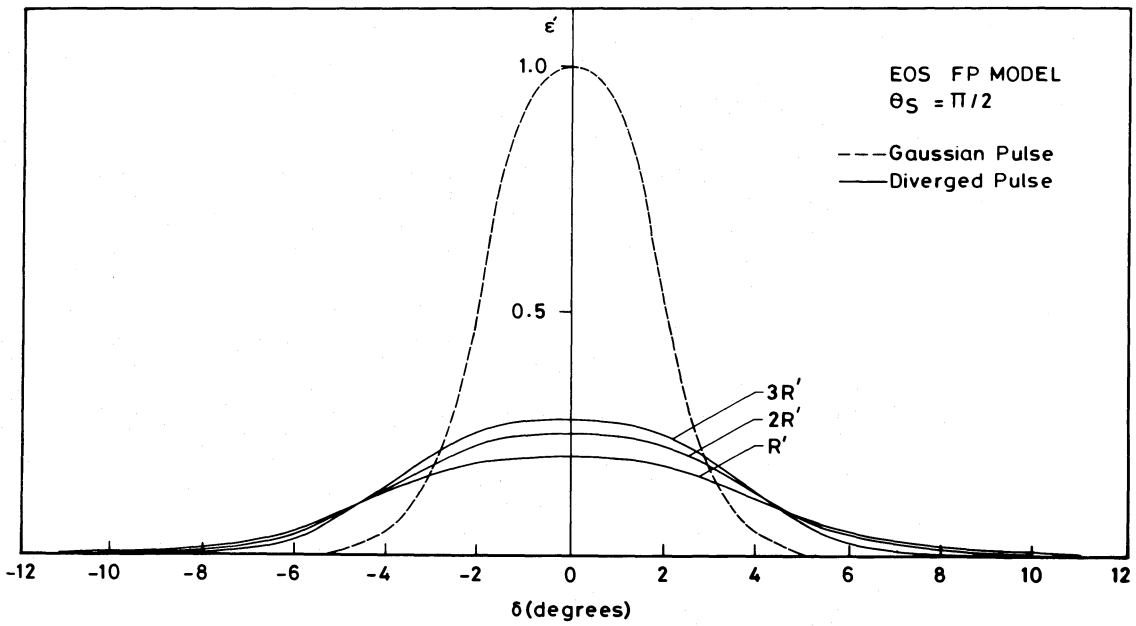

FIG. 3.—New deamplification factor ϵ' vs. azimuthal angle for $r_e = R', 2R', 3R'$ (*solid curves*). The dashed curve corresponds to the initial (Gaussian) profile.

Novikov 1971). This can be thought of as the relativistic analog of Faraday rotation. For emission along the polar axis, the amount of rotation of the plane of polarization (in the direction of the rotation of the pulsar) is

$$\int_{r_e}^{D} \omega \frac{dt}{dr}\, dr = \int_{r_e}^{D} \omega e^{-2\nu} dr \approx \frac{1}{2} r_e \omega(r_e)$$

and has a value of $\sim 1°$. The effect is quite small, and in the absence of a reference, is of academic interest only.

In Schwarzschild spacetime, photons emitted at $\pm\delta$ would take the same time to reach a remote observer. With the rotation of the neutron star, this symmetry will not be maintained. The backward-emitted (i.e., $\delta > 0$) photons will take a longer time to reach the observer than the forward-emitted (i.e., $\delta < 0$) photons. The difference in the arrival times of $\pm\delta$ photons, referred to as time delay, can be calculated from equation (34). It is largest for the equatorial photons and shows a consistent increase as the emission point is shifted away from the surface of the rotating neutron star. These are illustrated in Tables 7–9

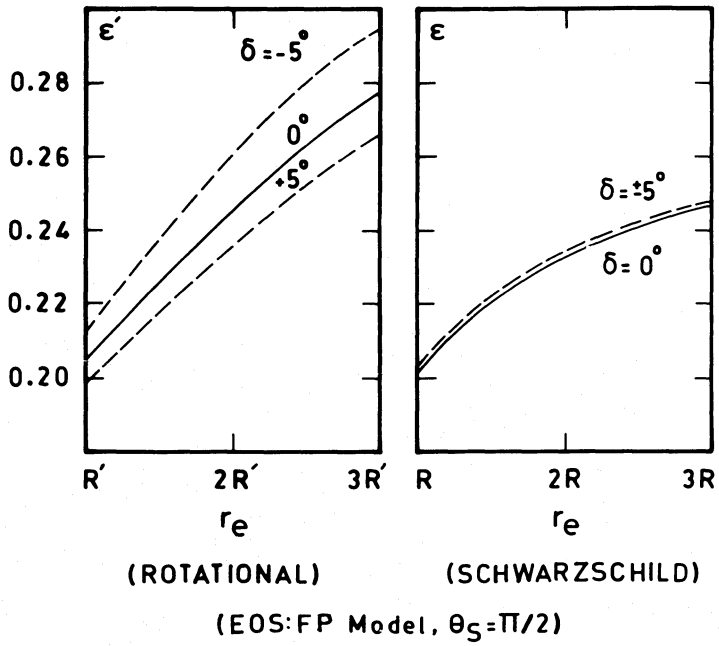

FIG. 4.—Net deamplification factor ϵ' vs. radial emission location r_e for various values of δ and for rotational and Schwarzschild cases

TABLE 7

$r_e = R'$

θ_s	v_s (c)	Pulse Tilt Angle	Time Delay for δ (μs) $\pm 1°$	$\pm 2°$	$\pm 3°$	$\pm 4°$	$\pm 5°$
RP Equation of State							
18°.....	0.044	9°.190	...	0.2	0.3	0.3	0.4
36.....	0.083	9.182	0.1	0.3	0.4	0.7	0.8
54.....	0.125	9.171	0.2	0.5	0.7	0.9	1.1
72.....	0.135	9.163	0.2	0.5	0.8	1.0	1.3
90.....	0.142	9.160	0.2	0.5	0.8	1.1	1.4
FP Equation of State							
18°.....	0.049	10°.276	0.1	0.2	0.3	0.4	0.5
36.....	0.093	10.270	0.2	0.4	0.5	0.8	0.9
54.....	0.128	10.262	0.2	0.5	0.7	1.0	1.2
72.....	0.151	10.256	0.3	0.6	0.9	1.2	1.5
90.....	0.158	10.253	0.3	0.6	1.0	1.3	1.5
CDK Equation of State							
18°.....	0.052	10°.896	0.1	0.2	0.3	0.4	0.6
36.....	0.099	10.892	0.2	0.4	0.7	0.8	1.0
54.....	0.135	10.886	0.3	0.5	0.8	1.1	1.3
72.....	0.160	10.882	0.3	0.6	1.0	1.3	1.7
90.....	0.168	10.880	0.3	0.6	1.0	1.3	1.7
BJ Equation of State							
18°.....	0.060	12°.552	0.2	0.2	0.4	0.5	0.6
36.....	0.114	12.557	0.2	0.5	0.5	1.0	1.2
54.....	0.157	12.563	0.3	0.7	1.0	1.4	1.7
72.....	0.185	12.568	0.4	0.8	1.2	1.6	1.9
90.....	0.194	12.570	0.4	0.8	1.3	1.6	2.1
TI Equation of State							
18°.....	0.077	15°.625	0.2	0.4	0.6	0.7	0.9
36.....	0.146	15.653	0.3	0.7	1.1	1.4	1.8
54.....	0.202	15.687	0.5	1.0	1.5	2.0	2.5
72.....	0.237	15.716	0.6	1.1	1.8	2.3	2.9
90.....	0.249	15.727	0.7	1.2	1.8	2.4	3.0

TABLE 8

$r_e = 2R'$

θ_s	v_s (c)	Pulse Tilt Angle	Time Delay for δ (μs) $\pm 1°$	$\pm 2°$	$\pm 3°$	$\pm 4°$	$\pm 5°$
RP Equation of State							
18°.....	0.093	18°.583	0.3	0.6	0.8	1.1	1.3
36.....	0.178	18.646	0.5	1.0	1.5	2.0	2.6
54.....	0.245	18.727	0.7	1.3	2.0	2.8	3.4
72.....	0.288	18.793	0.8	1.6	2.4	3.2	3.9
90.....	0.302	18.819	0.8	1.7	2.6	3.3	4.2
FP Equation of State							
18°.....	0.101	20°.008	0.3	0.6	0.9	1.3	1.6
36.....	0.193	20.092	0.6	1.2	1.7	2.3	2.9
54.....	0.265	20.199	0.8	1.6	2.4	3.1	3.9
72.....	0.319	20.288	0.9	1.9	2.8	3.6	4.6
90.....	0.328	20.322	1.0	1.9	2.8	3.9	4.7
CDK Equation of State							
18°.....	0.106	20°.866	0.3	0.6	1.0	1.3	1.7
36.....	0.202	20.964	0.7	1.3	1.9	2.5	3.1
54.....	0.278	21.090	0.8	1.7	2.6	3.5	4.3
72.....	0.327	21.194	1.0	2.0	3.0	4.0	4.9
90.....	0.343	21.235	1.1	2.0	3.1	4.2	5.2
BJ Equation of State							
18°.....	0.119	23°.010	0.5	0.8	1.3	1.7	2.0
36.....	0.226	23.144	0.8	1.6	2.3	3.1	3.9
54.....	0.311	23.329	1.0	2.1	3.1	4.2	5.2
72.....	0.365	23.434	1.2	2.4	3.6	4.8	5.9
90.....	0.384	23.545	1.3	2.5	3.7	5.0	6.2
TI Equation of State							
18°.....	0.150	28°.241	0.6	1.3	1.9	2.5	3.1
36.....	0.285	28.539	1.2	2.3	3.5	4.7	5.8
54.....	0.392	28.951	1.5	3.1	4.7	6.2	7.7
72.....	0.460	29.270	1.7	3.5	5.3	7.0	8.8
90.....	0.484	29.406	1.8	3.7	5.8	7.3	9.1

(for all the equations of state used here), which also contain the values of v_s, the emitter's tangential velocity as seen by a locally nonrotating observer.

Time delays would be larger if the cone angle were larger. If the time delay equals the pulse duration, the complete pulse will be detected by the observer. That is, by the time the emission cone sweeps past the observer, the photons at the largest positive value of δ will have just reached the detector. If, however, the time delay between the maximum and minimum values of δ exceeds the pulse duration, photons with values larger than a limiting value of δ will miss the detector. As a result, the pulse will have a gradual buildup but a steeper cutoff. This will be an additional contributory factor to the asymmetry in the final pulse profile (aside from the inertial frame drag effect and interstellar/planetary scintillation, if any), and will constrain the pulsar's duty cycle.

To summarize, the effects due to spacetime curvature make the pulse cone wider (by a factor of ~ 2) and the pulse intensity smaller (the peak gets reduced by a factor of ~ 5). The main effect of rotation is to introduce an asymmetry in the pulse profile; this effect, however, is comparatively smaller. These effects are purely general relativistic, and will be over and above any (frequency-dependent) effect on the propagation of electromagnetic waves (such as ray bending, absorption, etc.) through anisotropic/inhomogeneous magnetized plasma. Observationally, most pulsars show a narrow pulse profile. Our calculations would, therefore, suggest that at the emission location, the pulse starts out in the shape of a narrow spike. Since the brightness temperature of the source is directly proportional to the intensity of radiation, this would have an important implication, namely, the brightness temperatures of pulsars in general (since the curvature effects are dominant over the rotational effects) are larger by an order of magnitude (in the emitter's frame) than are presently presumed. In view of Figure 3, this statement will be valid for the emitter located anywhere between the pulsar surface and several times its radius.

Note added in manuscript.—Mention may be made here of calculations that take into account post-Newtonian effects on

TABLE 9

$r_e = 3R'$

θ_s	v_s (c)	Pulse Tilt Angle	Time Delay for δ (μs)				
			$\pm 1°$	$\pm 2°$	$\pm 3°$	$\pm 4°$	$\pm 5°$
RP Equation of State							
18°.....	0.137	26°.139	0.5	1.0	1.6	2.2	2.7
36.....	0.261	26.367	1.0	2.0	3.0	4.0	5.0
54.....	0.359	26.664	1.4	2.7	4.0	5.3	6.7
72.....	0.422	26.918	1.5	3.1	4.6	6.1	7.6
90.....	0.444	27.018	1.6	3.1	4.8	6.3	7.9
FP Equation of State							
18°.....	0.149	28°.143	0.7	1.3	1.9	2.5	3.2
36.....	0.283	28.437	1.2	2.3	3.5	4.7	5.8
54.....	0.389	28.823	1.5	3.1	4.6	6.1	7.7
72.....	0.458	29.157	1.8	3.5	5.2	6.9	8.7
90.....	0.481	29.290	1.8	3.6	5.4	7.2	9.1
CDK Equation of State							
18°.....	0.156	29°.369	0.7	1.4	2.0	2.8	3.4
36.....	0.297	29.710	1.3	2.5	3.7	5.1	6.3
54.....	0.408	30.161	1.6	3.3	5.0	6.6	8.3
72.....	0.480	30.554	1.9	3.8	5.7	7.6	9.4
90.....	0.505	30.711	1.9	3.9	5.8	7.8	9.7
BJ Equation of State							
18°.....	0.174	32°.478	0.8	1.7	2.5	3.4	4.2
36.....	0.332	32.911	1.6	3.1	4.6	6.1	7.6
54.....	0.456	33.565	2.1	4.0	6.0	8.0	10.0
72.....	0.536	34.147	2.2	4.3	6.7	8.9	11.2
90.....	0.564	34.385	2.4	4.6	6.9	9.2	11.5
TI Equation of State							
18°.....	0.220	40°.051	1.3	2.6	3.8	5.1	6.5
36.....	0.419	41.064	2.3	4.6	6.9	9.2	11.5
54.....	0.577	42.525	2.9	5.7	8.6	11.5	14.4
72.....	0.678	43.942	3.1	6.1	9.2	12.2	15.3
90.....	0.713	44.558	3.1	6.2	9.2	12.3	15.4

pulse arrival times. Epstein (1977), for example, has considered the gravitational propagation delay and post-Newtonian corrections to the elliptical binary orbit for PSR 1913+16, which may be useful in determining whether the observed periastron precession rate is entirely due to the general relativistic effects of compact mass. However, the pulse arrival time analysis is based on the assumption that the pulsar is an isotropic point source of energy, and so qualitative changes in the pulse profile due to rotationally induced dragging of inertial frames as discussed here are not manifest.

The neutron star structure parameters that we have used in this work are for the star on the verge of secular rotational instability (Ray and Datta 1984). The same quantities for the dynamical instability can easily be constructed by noting that the spherical deformations in mass and radius scale as Ω^2 for a given nonrotating set (M, R). The secular limit, rather than the dynamical one, is used because the former is a stronger restriction on the rotational speed, and if the millisecond pulsar is envisaged as a neutron star spun up, the secular instability intervenes earlier than the dynamical. Shapiro, Teukolsky, and Wasserman (1983) have considered published models of equilibrium spherical nonrotating stars that can be uniformly spun up to millisecond periods and will still remain in hydrostatic equilibrium. Their treatment is general relativistic and valid for arbitrarily fast rotations of a uniform density, centrally condensed Roche model, and suggests that PSR 1937+214 may be rotating a factor of 2 slower than the instability limit. The main conclusions reported here will, however, remain valid, since our calculations show that the effects of spacetime curvature dominate over those of rotation.

We thank Professors J. V. Narlikar, Ch. V. Sastry, V. Radhakrishnan, and our colleagues at the Raman Research Institute for helpful discussions. B. D. acknowledges the Indian National Science Academy for the award of a Biren Roy Trust Fellowship.

REFERENCES

Backer, D. C., Kulkarni, S. R., Heiles, C., Davis, M. M., and Goss, W. M. 1982, *Nature*, **300**, 615.
Boriakoff, V., Buccheri, R., and Fauci, F. 1983, *Nature*, **304**, 417.
Canuto, V., Datta, B., and Kalman, G. 1978, *Ap. J.*, **221**, 274 (CDK).
Datta, B., and Kapoor, R. C. 1985, *Nature*, **315**, 557.
Datta, B., and Ray, A. 1983, *M.N.R.A.S.*, **204**, 75P.
Epstein, R. 1977, *Ap. J.*, **216**, 92.
Friedman, B., and Pandharipande, V. R. 1981, *Nucl. Phys.*, **A361**, 502 (FP).
Hartle, J. B., and Thorne, K. S. 1968, *Ap. J.*, **153**, 807.
Joss, P. C., and Rappaport, S. 1984, *Ann. Rev. Astr. Ap.*, **22**, 537.
Kapoor, R. C., and Datta, B. 1984, *M.N.R.A.S.*, **209**, 895.
Pandharipande, V. R., Pines, D., and Smith, R. A. 1976, *Ap. J.*, **208**, 550.
Radhakrishnan, V., and Cooke, D. J. 1969, *Ap. Letters*, **3**, 225.
Ray, A., and Datta, B. 1984, *Ap. J.*, **282**, 542.
Shapiro, S. L., Teukolsky, S. A., and Wasserman, I. 1983, *Ap. J.*, **272**, 702.
Tassoul, J. L. 1978, *Theory of Rotating Stars* (Princeton: Princeton University Press).
Zeldovich, Ya. B., and Novikov, I. D. 1971, *Relativistic Astrophysics*, Vol. **1**, (Chicago: University of Chicago Press).

B. Datta and R. C. Kapoor: Indian Institute of Astrophysics, Bangalore 560 034, India